Computational Method for Non-Conservation Form of 1-D Unsteady Euler Equations for Closed-Loop Transport Systems

Nhan T. Nguyen*
NASA Ames Research Center
Moffett Field, CA 94035

This paper describes a modeling method for closed-loop unsteady fluid transport systems based on 1-D unsteady Euler equations with nonlinear forced periodic boundary conditions. A significant feature of this model is the incorporation of dynamic constraints on the variables that control the transport process at the system boundaries as they often exist in many transport systems. These constraints result in a coupling of the Euler equations with a system of ordinary differential equations that model dynamics of auxiliary processes connected to the transport system. Another important feature of the transport model is the use of the non-conservation form instead of the flux-conserved form. This form lends itself to modeling with measurable conserved fluid transport variables and represents an intermediate model between the primitive variable approach and the conserved variable approach. A wave-splitting finite-difference upwind method is presented as a numerical solution of the model. An iterative procedure is implemented to solve the nonlinear forced periodic boundary conditions prior to the time-marching procedure for the upwind method. A shock capturing method to handle transonic flow for the non-conservation form of the Euler equations is presented. A closed-loop wind tunnel is used for demonstration of the accuracy of this modeling method.

I. Introduction

A transport system is a system that carries information from one point to another point within the system. Examples of transport systems are numerous such as fluid flow in gas distribution pipelines,[1] air traffic systems,[2] highway traffic systems,[3] just to name a few. The underlying mathematical principle of a transport system is the hyperbolic partial differential equation which models such a system as a continuum whose information varies in space and time.[4] This equation is used to model a wave propagation behavior in many transport systems since information is carried from one point to another point within the continuum by wave actions. Associated with the hyperbolic partial differential equation are a number of boundary conditions that specify the configurations of these systems. If the information is carried in one direction without returning to its starting position, then we say that the system is open-loop. An example of an open-loop transport system is gas flow through an aircraft engine. On the other hand, if the information returns to its starting position, then the system is said to be closed-loop. An example of a closed-loop transport system is the circulatory system in a biological system. The flow of information is usually supplied at the system boundary by a forced process that provides a motive force to move the information along the way. A common device for accomplishing this objective in fluid transport systems is a pump which supplies a positive pressure wave to displace the fluid volume in the flow direction. In this study, we will focus on such a closed-loop fluid transport system that is energized by a positive-displacement device such as a turbomachinery compressor. While the focus is on a fluid transport system, the underlying principle is sufficiently general for other types of transport systems. This study is motivated by the need for modeling a closed-loop wind tunnel system which is a good example of a closed-loop transport system.

The paper presents the development of a computational hyperbolic model for a closed-loop fluid system based on the 1-D unsteady Euler equations. The hyperbolic model is an intermediate model between the conservation form and the non-conservation form that affords a certain advantage for continuous flow with dissipation and varying area. A nonlinear forced periodic boundary condition is imposed on the model to describe a forced process that generate the flow of information. This boundary condition in turn is coupled to a system of ordinary differential equations that

*Computer Scientist, Intelligent Systems Division, Mail Stop 269-1, AIAA Senior Member

represent dynamics of auxiliary systems that actually drive the information flow in the closed-loop system. We also present an explicit scheme of a wave-splitting, finite-difference upwind method for solving this hyperbolic model. The computational results for a closed-loop wind tunnel model show a very good agreement with experimental data.

II. Closed-Loop Transport Model

A. Hyperbolic Equations in Non-Conservation Form

Fluid transport phenomena are governed by the conservation laws of mass, momentum, and energy. These equations are hyperbolic in nature. For 1-D internal flow, the governing unsteady Euler equations are expressed in a conservation form as[5]

$$\frac{\partial \mathbf{U}}{\partial t} + \frac{\partial \mathbf{F}\left(\mathbf{U}, x\right)}{\partial x} + \mathbf{Q}\left(\mathbf{U}, x\right) = \mathbf{0} \qquad \forall x \in [0, L], t \in [0, T] \tag{1}$$

where $\mathbf{U}\left(x,t\right) : [0,L] \times [0,T] \rightarrow \mathbb{R}^n$ is a vector of transport variables with $n = 3$, $\mathbf{F}\left(\mathbf{U}, x\right)$ is a flux vector of conserved quantities, and $\mathbf{Q}\left(\mathbf{U}, x\right)$ is non-homogeneous dissipative source term. In the vector form, $\mathbf{U}$, $\mathbf{F}$, and $\mathbf{Q}$ are defined as

$$\mathbf{U}\left(x,t\right) = \begin{bmatrix} \rho A \\ \rho u A \\ \rho A c_v T + \frac{1}{2}\rho u^2 A \end{bmatrix}, \ \mathbf{F}\left(\mathbf{U}, x\right) = \begin{bmatrix} \rho u A \\ \rho u^2 A + pA \\ \rho u A c_p T + \frac{1}{2}\rho u^3 A \end{bmatrix}, \ \mathbf{Q}\left(\mathbf{U}, x\right) = \begin{bmatrix} 0 \\ -p\frac{dA}{dx} + \frac{1}{2}\rho u^2 A \frac{f}{D} \\ -\frac{dQ}{dx} \end{bmatrix} \tag{2}$$

where ρ is the density, p is the pressure, u is the flow speed, T is the temperature, $A(x)$ is the varying flow area, f is the friction factor, D is the hydraulic diameter, $\frac{dQ}{dx}$ is the heat transfer gradient, c_v is the constant-volume specific heat, and c_p is the constant-pressure specific heat.

Equation (1) admits a continuous solution as well as a discontinuous solution that describes the evolution of a shock discontinuity which requires Eq. (1) to be cast in a weak form in order to handle the infinite spatial derivative of the flux vector through the shock. The weak form solution relates the information on either side of the discontinuity by the integral form of Eq. (1) which results in the well-known Rankine-Hugoniot relations.[6]

Suppose the vector $\mathbf{U}$ can be expressed as a function of some flow variables $\mathbf{y}$ so that

$$\mathbf{U}\left(x,t\right) = \mathbf{U}\left(\mathbf{y}\left(x,t\right)\right) \tag{3}$$

Then by explicit differentiation, Eq. (1) can be rewritten in a non-conservation form as

$$\frac{\partial \mathbf{y}}{\partial t} + \mathbf{A}\left(\mathbf{y}, x\right)\frac{\partial \mathbf{y}}{\partial x} + \mathbf{B}\left(\mathbf{y}, x\right) = \mathbf{0} \tag{4}$$

where $\mathbf{A}\left(\mathbf{y}, x\right) : \mathbb{R}^n \times [0, L] \rightarrow \mathbb{R}^n \times \mathbb{R}^n$ is a characteristic matrix and $\mathbf{B}\left(\mathbf{y}, x\right) : \mathbb{R}^n \times [0, L] \rightarrow \mathbb{R}^n$ is a non-homogeneous dissipative source term such that

$$\mathbf{A} = \left(\frac{\partial \mathbf{U}}{\partial \mathbf{y}}\right)^{-1}\left(\frac{\partial \mathbf{F}}{\partial \mathbf{U}}\right)\left(\frac{\partial \mathbf{U}}{\partial \mathbf{y}}\right) \tag{5}$$

$$\mathbf{B} = \left(\frac{\partial \mathbf{U}}{\partial \mathbf{y}}\right)^{-1}\left(\frac{\partial \mathbf{F}}{\partial x} + \mathbf{Q}\right) \tag{6}$$

Equation (4) is a system of first order, quasilinear strictly hyperbolic equations due to the fact that the matrix $\mathbf{A}$ has n real, distinct eigenvalues such that

$$\lambda_1\left(\mathbf{A}\right) < \lambda_2\left(\mathbf{A}\right) < \cdots < \lambda_n\left(\mathbf{A}\right) \tag{7}$$

for all $\mathbf{y}\left(x,t\right) \in \mathbb{R}^n$, $x \in [0, L]$, and $t \in [0, T]$. Under this condition, the matrix $\mathbf{A}$ is diagonalizable using a similarity transformation

$$\mathbf{A} = \mathbf{\Phi}\mathbf{\Lambda}\mathbf{\Phi}^{-1} \tag{8}$$

where $\mathbf{\Phi}$ is an matrix of the right eigenvectors and $\mathbf{\Lambda}$ is a diagonal matrix of the right eigenvalues of $\mathbf{A}$

$$\mathbf{\Lambda} = \begin{bmatrix} u+c & 0 & 0 \\ 0 & u & 0 \\ 0 & 0 & u-c \end{bmatrix} \tag{9}$$

with c as the speed of sound.

The eigenvalues are the acoustic wave speeds of the fluid transport systems and the direction of the wave propagation is called a characteristic direction. For subsonic transport, the information in the fluid medium is carried in both the upstream and downstream directions by one upstream wave speed $u - c$ and two downstream wave speeds u and $u + c$. Since $x \in [0, L]$, then for the information to be transported in the upstream direction, data must exist at the boundary $x = L$. Similarly, data must also exist at the boundary $x = 0$ in order for information to be carried downstream in the flow. The number of upstream and downstream boundary conditions must match the number of upstream and downstream wave speeds. This is known as the boundary condition compatibility.

Premultiplying Eq. (4) by $\mathbf{\Phi}^{-1}$, we obtain the characteristic form of the hyperbolic partial differential equation

$$\mathbf{\Phi}^{-1}\mathbf{y}_t + \mathbf{\Lambda}\mathbf{\Phi}^{-1}\mathbf{y}_x + \mathbf{\Phi}^{-1}\mathbf{B} = \mathbf{0} \tag{10}$$

Equations (1) and (4) are completely equivalent, but there are significant differences in the numerical implementation of these equations. The conservation form of Eq. (1) yields a solution that is conserved throughout the domain of x, resulting in a correct steady state solution. For example, examining the first row of Eq. (1), it is clear that the steady state solution requires that the mass flux variable $\rho u A$ be constant with respect to x. This is a well-known result in fluid mechanics. In the numerical implementation, this mass flux conservation is incorporated directly into the solution method in order to guarantee that the general time unsteady solution will converge to the correct steady state solution.[7]

On the other hand, the hyperbolic non-conservation form of Eq. (4) can take on a wide range of expressions, some of which are more advantageous than others from a numerical implementation standpoint. For example, one common non-conservation form of Eq. (4) is

$$\frac{\partial}{\partial t}\begin{bmatrix} p \\ u \\ c^2 \end{bmatrix} + \begin{bmatrix} u & \gamma p & 0 \\ \frac{c^2}{\gamma p} & u & 0 \\ 0 & (\gamma-1)\,c^2 & u \end{bmatrix} \frac{\partial}{\partial x}\begin{bmatrix} p \\ u \\ c^2 \end{bmatrix} + \begin{bmatrix} \gamma p u \frac{dA}{Adx} - \frac{(\gamma-1)\gamma p u^3}{2c^2}\frac{f}{D} - \frac{\gamma-1}{A}\frac{dQ}{dx} \\ \frac{u^2}{2}\frac{f}{D} \\ (\gamma-1)\,c^2 u \frac{dA}{Adx} - \frac{(\gamma-1)\gamma u^3}{2}\frac{f}{D} - \frac{(\gamma-1)c^2}{pA}\frac{dQ}{dx} \end{bmatrix} = \begin{bmatrix} 0 \\ 0 \\ 0 \end{bmatrix} \tag{11}$$

where γ is the specific heat ratio. In this form, the variables p, u, and c^2 are called primitive variables or basic variables.

The right eigenvector matrix $\mathbf{\Phi}$ for Eq. (11) is computed as

$$\mathbf{\Phi} = \begin{bmatrix} \frac{\gamma p}{(\gamma-1)c^2} & 0 & \frac{\gamma p}{(\gamma-1)c^2} \\ \frac{1}{(\gamma-1)c} & 0 & -\frac{1}{(\gamma-1)c} \\ 1 & 1 & 1 \end{bmatrix} \tag{12}$$

Then the characteristic form of Eq. (11) becomes

$$\begin{bmatrix} \frac{(\gamma-1)c^2}{2\gamma p}\frac{\partial p}{\partial t} + \frac{(\gamma-1)c}{2}\frac{\partial u}{\partial t} \\ -\frac{(\gamma-1)c^2}{\gamma p}\frac{\partial p}{\partial t} + \frac{\partial c^2}{\partial t} \\ \frac{(\gamma-1)c^2}{2\gamma p}\frac{\partial p}{\partial t} - \frac{(\gamma-1)c}{2}\frac{\partial u}{\partial t} \end{bmatrix} + \begin{bmatrix} u+c & 0 & 0 \\ 0 & u & 0 \\ 0 & 0 & u-c \end{bmatrix} \begin{bmatrix} \frac{(\gamma-1)c^2}{2\gamma p}\frac{\partial p}{\partial x} + \frac{(\gamma-1)c}{2}\frac{\partial u}{\partial x} \\ -\frac{(\gamma-1)c^2}{\gamma p}\frac{\partial p}{\partial x} + \frac{\partial c^2}{\partial x} \\ \frac{(\gamma-1)c^2}{2\gamma p}\frac{\partial p}{\partial x} - \frac{(\gamma-1)c}{2}\frac{\partial u}{\partial x} \end{bmatrix}$$
$$+ \begin{bmatrix} \frac{(\gamma-1)c^2 u}{2}\frac{dA}{Adx} + \frac{(\gamma-1)c^2u^2 - (\gamma-1)^2cu^3}{4c}\frac{f}{D} - \frac{(\gamma-1)^2c^2}{2\gamma pA}\frac{dQ}{dx} \\ -\frac{(\gamma-1)u^3}{2}\frac{f}{D} - \frac{(\gamma-1)c^2}{\gamma pA}\frac{dQ}{dx} \\ \frac{(\gamma-1)c^2 u}{2}\frac{dA}{Adx} - \frac{(\gamma-1)c^2u^2 + (\gamma-1)^2cu^3}{4c}\frac{f}{D} - \frac{(\gamma-1)^2c^2}{2\gamma pA}\frac{dQ}{dx} \end{bmatrix} = \begin{bmatrix} 0 \\ 0 \\ 0 \end{bmatrix} \tag{13}$$

The three characteristic directions are defined by $\left(\frac{dx}{dt}\right)_{1,2,3} = u \pm c, u$ such that on these characteristic directions, the total derivative of a quantity is computed as

$$\left(\frac{d}{dt}\right)_i = \frac{\partial}{\partial t} + \left(\frac{dx}{dt}\right)_i \frac{\partial}{\partial x} \tag{14}$$

where $i = 1, 2, 3$ denotes the characteristic direction.

Therefore, we can write out Eq. (13) as

$$\frac{c}{\gamma p}\left(\frac{dp}{dt}\right)_{1,2} \pm \left(\frac{du}{dt}\right)_{1,2} + cu\frac{dA}{Adx} \pm \frac{cu^2 \mp (\gamma-1)\,u^3}{2c}\frac{f}{D} - \frac{(\gamma-1)\,c}{\gamma pA}\frac{dQ}{dx} = 0 \tag{15}$$

$$-\frac{1}{p}\left(\frac{dp}{dt}\right)_3 + \frac{\gamma}{(\gamma-1)\,c^2}\left(\frac{dc^2}{dt}\right)_3 - \frac{\gamma u^3}{2c^2}\frac{f}{D} - \frac{1}{pA}\frac{dQ}{dx} = 0 \tag{16}$$

We recall that the entropy of a perfect gas is defined as

$$ds = \frac{\gamma R}{\gamma-1}\frac{dT}{T} - R\frac{dp}{p} = R\left(\frac{\gamma}{\gamma-1}\frac{dc^2}{c^2} - \frac{dp}{p}\right) \tag{17}$$

Then, substituting Eq. (17) into Eq. (16) yields

$$\left(\frac{ds}{dt}\right)_3 = \frac{u^3}{2T}\frac{f}{D} + \frac{1}{\rho TA}\frac{dQ}{dx} \geq 0 \tag{18}$$

From Eq. (15), it can be seen that the pressure and flow speed propagate at wave speeds $u \pm c$, while Eq. (18) shows that the entropy propagates at a wave speed u. Equation (18) also implies an important thermodynamic property that, for an adiabatic flow, the friction factor must be positive to ensure that entropy change is positive according to the second law of thermodynamics. For a perfect gas, the isentropic relationship between the density and pressure is expressed as

$$\frac{\rho}{\rho_0} = \left(\frac{p}{p_0}\right)^{\frac{1}{k}} \tag{19}$$

We substitute Eq. (19) into Eq. (15) and then integrate the resulting equation along with Eq. (18). Upon simplification, we get

$$\left(u \pm \frac{2c}{\gamma-1}\right)_{1,3} = \int\left[\mp cu\frac{dA}{Adx} - \frac{cu^2 \mp (\gamma-1)\,u^3}{2c}\frac{f}{D} \pm \frac{(\gamma-1)\,c}{\gamma pA}\frac{dQ}{dx}\right]dt \tag{20}$$

$$(s)_2 = \int R\left(\frac{\gamma u^3}{2c^2}\frac{f}{D} + \frac{1}{pA}\frac{dQ}{dx}\right)dt \tag{21}$$

For inviscid, adiabatic flow with a constant area, we see that the integral terms in the right hand sides of Eqs. (20) and (21) vanish, thus rendering the expressions on the left hand sides constant. As a result, the expressions on the right hand sides $u \pm \frac{2c}{k-1}$ and s are the well-known Riemann invariants which are conserved along the characteristic directions $\left(\frac{dx}{dt}\right)_{1,2,3} = u \pm c, u$ for inviscid, adiabatic flow.[6] For viscous flow, these Riemann invariants are no longer conserved along the characteristic directions. However, the Riemann invariant concept is important in studying shock capturing methods that involve discontinuous solutions.

The conservation form of Eq. (1) is very popular in computational fluid dynamics because it addresses the conservation laws directly for flow with shock discontinuities. On the other hand, the hyperbolic non-conservation form of Eq. (4) using the primitive variables such as Eq. (11) in general does not necessarily preserve the conservation features of the transport physics because the flux variables as reconstructed from the primitive variables may not be necessarily conserved. However, the advantage of using conservation form is not without a trade-off. The fact that the momentum flux variable is usually not a directly measurable quantity can potentially result in an increased complexity in formulating numerical methods for certain physical applications wherein the boundary conditions are specified in terms of directly measurable quantities.

From Eq. (1), we note that the mass flux variable is the same as the mass flow $\dot{m} = \rho uA$ in a 1-D flow, and the energy flux variable takes on the meaning of the enthalpy $\dot{m}c_pT_0$ of the fluid, where T_0 is the stagnation temperature. Since the mass flow is always conserved, the stagnation temperature therefore is also conserved for an adiabatic process and thus is proportional to the energy flux variable. On the other hand, the momentum flux variable is generally not conserved for shock free, inviscid flow with a varying area. Instead, we can replace the momentum flux variable with the stagnation pressure p_0 as a variable that is generally conserved for shock free, inviscid flow. Thus, this leads

us to consider the following hyperbolic form in terms of the mass flow, the stagnation pressure, and the stagnation temperature

$$\frac{\partial}{\partial t}\begin{bmatrix}\dot{m}\\ p_0\\ T_0\end{bmatrix}+\begin{bmatrix}u & \frac{pA}{p_0} & \frac{\dot{m}u}{2T_0}\\ \frac{\rho_0 c^2}{\rho A} & u\left[1-\frac{(\gamma-1)T}{T_0}\right] & \frac{\rho_0 c^2 u}{T_0}\\ \frac{(\gamma-1)T}{\rho A} & -\frac{(\gamma-1)^2 uT}{\gamma p_0} & u\left[1+\frac{(\gamma-1)T}{T_0}\right]\end{bmatrix}\frac{\partial}{\partial x}\begin{bmatrix}\dot{m}\\ p_0\\ T_0\end{bmatrix}$$
$$+\begin{bmatrix}\frac{\dot{m}u}{2}\frac{f}{D}\\ \frac{\rho_0 u^3}{2}\left(\frac{T_0}{T}-\gamma+1\right)\frac{f}{D}-\frac{\rho_0 c^2 u\left(2-M^2\right)}{2\dot{m}c_p T}\frac{dQ}{dx}\\ -(\gamma-1)uT\frac{f}{D}\left(\frac{T_0}{T}-1\right)-\frac{\gamma u}{\dot{m}c_p}\frac{dQ}{dx}\end{bmatrix}=\begin{bmatrix}0\\0\\0\end{bmatrix} \tag{22}$$

where ρ_0 is the stagnation density and M is the Mach number.

Equation (22) represents an intermediate model between the conservation form of Eq. (1) and the hyperbolic non-conservation form with primitive variables as in Eq. (11). In this form, the steady state solution is governed by the following equation

$$\frac{d\mathbf{y}}{dx}=-\mathbf{C}\left(\mathbf{y},x\right) \tag{23}$$

where

$$\mathbf{C}\left(\mathbf{y},x\right)=\mathbf{A}^{-1}\left(\mathbf{y},x\right)\mathbf{B}\left(\mathbf{y},x\right)=\begin{bmatrix}0\\ \frac{\gamma p_0 M^2}{2}\left(\frac{f}{D}+\frac{1}{\dot{m}c_p T_0}\frac{dQ}{dx}\right)\\ -\frac{1}{\dot{m}c_p}\frac{dQ}{dx}\end{bmatrix} \tag{24}$$

It is obvious from Eq. (23) that the mass flow is identically conserved along the x direction. For fluid transport without friction and heat transfer, the stagnation pressure and stagnation temperature are also conserved along the x direction. The eigenvalues of the matrix $\mathbf{A}$ in both Eqs. (11) and (22) are equal to the values in Eq. (9), thus demonstrating the invariant transformation of these equations. Equation (22) affords a certain advantage over the conservation form of Eq. (1) for subsonic flow in that it uses measurable quantities as variables from the boundary conditions that can significantly simplify computational methods.

B. Forced Periodic Boundary Conditions and Dynamic Constraints

In a closed-loop transport system, information is carried from one point to another point and then returned back to the starting position as illustrated in Fig. 1. To enable this information recirculation, a positive-displacement device must be embedded at the boundaries of the system. For subsonic transport, two boundary conditions at $x=0$ and one boundary condition at $x=L$ are required. For supersonic transport, three boundary conditions at $x=0$ are required. For a closed-loop system, the boundary conditions at $x=0$ are affected by the boundary conditions at $x=L$ since the information must be returned to its starting position. Thus, in general for a closed-loop system, we consider the following nonlinear forced periodic boundary condition for Eq. (4)

$$\mathbf{y}\left(0,t\right)=\mathbf{g}\left(\mathbf{y}\left(L,t\right),\mathbf{u}\right)\qquad\forall t\in[0,T] \tag{25}$$

where $\mathbf{u}\left(t\right):[0,T]\rightarrow\mathbb{R}^m$ in class C^1 is a boundary control vector, and $\mathbf{g}\left(\mathbf{y}\left(L,t\right),\mathbf{u}\right):\mathbb{R}^n\times\mathbb{R}^m\rightarrow\mathbb{R}^n$ is a forcing function that relates the transport state vectors at $x=0$ and $x=L$ and the boundary control vector $\mathbf{u}$. For a well-posed problem, we require that the boundary condition (25) be non-characteristic such that $\mathbf{g}\left(\mathbf{y}\left(L,t\right),\mathbf{u}\right)$ is nowhere tangential to any of the characteristic curves of Eq. (10).

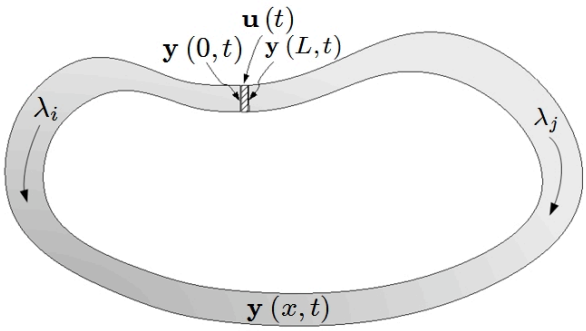

Fig. 1 - Closed-Loop Transport System

To ensure the boundary condition compatibility for all signs of the eigenvalues of $\mathbf{A}$, the Jacobian of $\mathbf{g}$ with respect to $\mathbf{y}(L,t)$ is required to be full rank or

$$\dim \frac{\partial \mathbf{g}}{\partial \mathbf{y}(L,t)} = n \tag{26}$$

where $n = 3$ is the number of the eigenvalues.

To see this, we let n^+ and n^- be the numbers of the positive and negative eigenvalues, respectively. If $n^+ = n$, the from Eq. (25), there are n^+ independent boundary conditions for $\mathbf{y}(0,t)$ that correspond to n^+ positive eigenvalues. Thus, the compatibility for the positive eigenvalues is satisfied. If $n^- = n$, then from Eqs. (25) and (26), there are n^- independent boundary conditions with $\mathbf{y}(L,t)$ that correspond to n^- negative eigenvalues. The compatibility for the negative eigenvalues is thus satisfied. If $0 < n^+ < n$, we choose n^+ independent boundary conditions with $\mathbf{y}(0,t)$ corresponding to n^+ positive eigenvalues. Then, From (26), there are n^- remaining boundary conditions with $\mathbf{y}(L,t)$ corresponding to n^- negative eigenvalues. Thus, the compatibility for the mixed-sign eigenvalues is satisfied.

The boundary condition (25) provides a control action to maintain the flow of information in a closed-loop system by the boundary control vector $\mathbf{u}$. In practice, the boundary control vector $\mathbf{u}$ ends up being controlled by an auxiliary process that dictates dynamic constraints on the boundary control action. Therefore, in general, we consider the dynamic constraints on the boundary control in Eq. (25) to be governed by a system of ordinary differential equations as follows

$$\dot{\mathbf{u}} = \mathbf{f}(\mathbf{y}(0,t), \mathbf{y}(L,t), \mathbf{u}, \mathbf{v}) \qquad \forall t \in [0,T] \tag{27}$$

where $\mathbf{v}(t) \in L^2[0,T] \rightarrow \mathbb{R}^l$ is an auxiliary control vector and $\mathbf{f}(\mathbf{y}(0,t), \mathbf{y}(L,t), \mathbf{u}, \mathbf{v}) : \mathbb{R}^n \times \mathbb{R}^n \times \mathbb{R}^m \times \mathbb{R}^l \rightarrow \mathbb{R}^m$ is a transition function of the auxiliary process.

Equation (27) describes the time-varying process of the boundary control as influenced by the dynamics of the auxiliary process encapsulated by the transition function $\mathbf{f}$ and the auxiliary control vector $\mathbf{v}$. The coupling with Eq. (1) is due to the existence of the transport state vectors $\mathbf{y}(0,t)$ and $\mathbf{y}(L,t)$ at the system boundaries.

To completely describe the problem, both Eqs. (4) and (27) are given the following initial conditions

$$\mathbf{y}(x,0) = \mathbf{h}(x) \tag{28}$$

$$\mathbf{u}(0) = \mathbf{u}_0 \tag{29}$$

where $\mathbf{h}$ is the steady state solution of Eq. (23) at the initial time. For a well-posed mixed initial-boundary value problem, the initial conditions (28) and (29) must be compatible with the boundary condition (25) such that

$$\mathbf{h}(0) = \mathbf{g}(\mathbf{h}(L), \mathbf{u}_0) \tag{30}$$

The problem is now posed as follows: given a closed-loop transport system initially at an equilibrium defined by the steady state solution $\mathbf{h}(x)$, we would like to adjust the auxiliary control $\mathbf{v}(t)$ so as to move the system to a new equilibrium at some later time. We are interested in the evolution of the fluid transport properties during this process.

III. Computational Method

Computation methods for hyperbolic partial differential equations are generally based on a finite-difference approach. There are several methods of spatial discretization used in finite difference methods that are designed to address numerical requirements of consistency, stability, and convergence. Briefly, the consistency requirement expresses that the discretized equations should tend to the differential equations to which they are related when Δt and Δx tend to zero. The stability requirement states that solutions must be bounded from one time step to another. The convergence requirement asserts that numerical solutions should approach their exact solutions throughout the solution domains when Δt and Δx tend to zero. For a well-posed mixed initial-boundary value problem, stability is the necessary and sufficient condition for convergence.[8]

A. Wave-Splitting Upwind Scheme

The simplest type of spatial discretization for a first-order, hyperbolic PDE is the first-order upwind finite-difference method. In flow with shocks, spatial discretization may not have sufficient stability requirements and could cause numerical oscillations at the discontinuities. Various spatial discretization schemes such as the Lax-Wendroff method incorporate an artificial viscosity to dampen these numerical oscillations. For the conservation laws with the dissipative source term $\mathbf{B}$ in Eq. (4), the friction factor f provides a natural viscosity for the numerical solutions so that an artificial viscosity may not be needed. From Eq. (9), we see that the eigenvalue $u - c$ is positive for supersonic flow and negative for subsonic flow. Thus for supersonic flow, Eq. (4) can be readily solved using the positive-wave upwind finite-difference method. For subsonic flow, however, we employ a wave-splitting, upwind finite-difference method to account for the mixed-sign eigenvalues.

For mixed-sign eigenvalues when $u < c$, the matrix $\mathbf{A}$ can also be splitted into a semi-positive definite matrix and a semi-negative definite matrix as

$$\mathbf{A} = \mathbf{A}^+ + \mathbf{A}^- \tag{31}$$

where

$$\mathbf{A}^+ = \mathbf{\Phi}\mathbf{\Lambda}^+\mathbf{\Phi}^{-1} \tag{32}$$

$$\mathbf{A}^- = \mathbf{\Phi}\mathbf{\Lambda}^-\mathbf{\Phi}^{-1} \tag{33}$$

with

$$\mathbf{\Lambda}^+ = \begin{bmatrix} u+c & 0 & 0 \\ 0 & u & 0 \\ 0 & 0 & 0 \end{bmatrix} \geq \mathbf{0} \qquad \forall t \in [0, T] \tag{34}$$

$$\mathbf{\Lambda}^- = \begin{bmatrix} 0 & 0 & 0 \\ 0 & 0 & 0 \\ 0 & 0 & u-c \end{bmatrix} \leq \mathbf{0} \qquad \forall t \in [0, T] \tag{35}$$

The characteristic equation (10) can be written in a wave-splitting form as

$$\mathbf{\Phi}^{-1}\mathbf{y}_t + \mathbf{\Lambda}^+\mathbf{\Phi}^{-1}\mathbf{y}_x + \mathbf{\Lambda}^-\mathbf{\Phi}^{-1}\mathbf{y}_x + \mathbf{\Phi}^{-1}\mathbf{B} = \mathbf{0} \tag{36}$$

Equation (36) is now discretized using a wave-splitting, first-order upwind finite-difference method as

$$\mathbf{\Phi}^{-1}\dot{\mathbf{y}}_i + \mathbf{\Lambda}^+\mathbf{\Phi}^{-1}\frac{\mathbf{y}_i - \mathbf{y}_{i-1}}{\Delta x} + \mathbf{\Lambda}^-\mathbf{\Phi}^{-1}\frac{\mathbf{y}_{i+1} - \mathbf{y}_i}{\Delta x} + \mathbf{\Phi}^{-1}\mathbf{B} = \mathbf{0} \tag{37}$$

where $i = 2, 3, \ldots, m-1$ denotes the index of the interior points not on the boundary such that $x_i = \frac{i-1}{m-1}L$ and $\mathbf{y}_i(t) = \mathbf{y}(x_i, t)$.

The following question is posed: at what grid point do we want to evaluate $\mathbf{\Phi}^{-1}$, $\mathbf{\Lambda}^+$, $\mathbf{\Lambda}^-$, and $\mathbf{B}$? To help answer this question, we examine the discretized form of the steady state equation (23) using a first-order spatial discretization

$$\mathbf{A}(\mathbf{y}_{i-1}, x_{i-1})\frac{\mathbf{y}_i - \mathbf{y}_{i-1}}{\Delta x} + \mathbf{B}(\mathbf{y}_{i-1}, x_{i-1}) = \mathbf{0} \tag{38}$$

This form is an explicit spatial discretization which yields a simple method for computing the steady state solution of Eq. (23). We see that $\mathbf{A}$ and $\mathbf{B}$ are evaluated at a prior grid point with respect to the discretization of $\mathbf{y}_x$. In order for

Eq. (37) to converge to the steady state solution based on the discretization scheme in Eq. (38), we need to maintain a numerical consistency between the steady state form and the hyperbolic form. This is done by evaluating all the matrices in Eq. (37) at a prior grid point for the positive wave speeds and at a current grid point for the negative wave speed. Using this approach, Eq. (37) can be decomposed into scalar equations as

$$\boldsymbol{\Psi}_1\left(\mathbf{y}_{i-1}, x_{i-1}\right)\dot{\mathbf{y}}_i + \left(u_{i-1}+c_{i-1}\right)\boldsymbol{\Psi}_1\left(\mathbf{y}_{i-1}, x_{i-1}\right)\frac{\mathbf{y}_i-\mathbf{y}_{i-1}}{\Delta x} + \boldsymbol{\Psi}_1\left(\mathbf{y}_{i-1}, x_{i-1}\right)\mathbf{B}\left(\mathbf{y}_{i-1}, x_{i-1}\right) = 0 \tag{39}$$

$$\boldsymbol{\Psi}_2\left(\mathbf{y}_{i-1}, x_{i-1}\right)\dot{\mathbf{y}}_i + u_{i-1}\boldsymbol{\Psi}_2\left(\mathbf{y}_{i-1}, x_{i-1}\right)\frac{\mathbf{y}_i-\mathbf{y}_{i-1}}{\Delta x} + \boldsymbol{\Psi}_2\left(\mathbf{y}_{i-1}, x_{i-1}\right)\mathbf{B}\left(\mathbf{y}_{i-1}, x_{i-1}\right) = 0 \tag{40}$$

$$\boldsymbol{\Psi}_3\left(\mathbf{y}_i, x_i\right)\dot{\mathbf{y}}_i + \left(u_i-c_i\right)\boldsymbol{\Psi}_3\left(\mathbf{y}_i, x_i\right)\frac{\mathbf{y}_{i+1}-\mathbf{y}_i}{\Delta x} + \boldsymbol{\Psi}_3\left(\mathbf{y}_i, x_i\right)\mathbf{B}\left(\mathbf{y}_i, x_i\right) = 0 \tag{41}$$

where $\boldsymbol{\Psi}_k\left(\mathbf{y}_i, x_i\right)$, $k = 1, 2, 3$, is the k-th 1×3 row vector of the matrix $\boldsymbol{\Phi}^{-1}\left(\mathbf{y}_i, x_i\right)$.

We now combine Eqs. (39) to (41) into a vector form as

$$\dot{\mathbf{y}}_i + \mathbf{A}_{i-1}^{+}\frac{\mathbf{y}_i-\mathbf{y}_{i-1}}{\Delta x} + \mathbf{A}_i^{-}\frac{\mathbf{y}_{i+1}-\mathbf{y}_i}{\Delta x} + \mathbf{B}_{i-1}^{+} + \mathbf{B}_i^{-} = \mathbf{0} \tag{42}$$

with

$$\mathbf{A}_{i-1}^{+} = \boldsymbol{\Psi}^{-1}\boldsymbol{\Lambda}^{+}\left(\mathbf{y}_{i-1}, x_{i-1}\right)\boldsymbol{\Psi} \tag{43}$$

$$\mathbf{A}_i^{-} = \boldsymbol{\Psi}^{-1}\boldsymbol{\Lambda}^{-}\left(\mathbf{y}_i, x_i\right)\boldsymbol{\Psi} \tag{44}$$

$$\mathbf{B}_{i-1}^{+} = \boldsymbol{\Psi}^{-1}\begin{bmatrix} \boldsymbol{\Psi}_1\left(\mathbf{y}_{i-1}, x_{i-1}\right)\mathbf{B}\left(\mathbf{y}_{i-1}, x_{i-1}\right) \\ \boldsymbol{\Psi}_2\left(\mathbf{y}_{i-1}, x_{i-1}\right)\mathbf{B}\left(\mathbf{y}_{i-1}, x_{i-1}\right) \\ 0 \end{bmatrix}_{3\times 1} \tag{45}$$

$$\mathbf{B}_i^{-} = \boldsymbol{\Psi}^{-1}\begin{bmatrix} 0 \\ 0 \\ \boldsymbol{\Psi}_3\left(\mathbf{y}_i, x_i\right)\mathbf{B}\left(\mathbf{y}_i, x_i\right) \end{bmatrix}_{3\times 1} \tag{46}$$

where

$$\boldsymbol{\Psi} = \begin{bmatrix} \boldsymbol{\Psi}_1\left(\mathbf{y}_{i-1}, x_{i-1}\right) \\ \boldsymbol{\Psi}_2\left(\mathbf{y}_{i-1}, x_{i-1}\right) \\ \boldsymbol{\Psi}_3\left(\mathbf{y}_i, x_i\right) \end{bmatrix}_{3\times 3} \tag{47}$$

We note that in general wave-splitting schemes are less conservative than flux-splitting schemes which better preserve the conservation laws across shock waves. However, for continuous subsonic flow, the wave splitting schemes can yield good results. In particular, the wave-splitting scheme in Eq. (42) ensures that the time evolution of the hyperbolic solution will converge to the correct steady state solution if it is also discretized in the same manner. Comparing this method of wave-splitting scheme with a well-known scheme, the difference is that the matrices $\mathbf{A}_{i-1}^{+}$ and $\mathbf{A}_i^{-}$ are evaluated at a prior grid point for the positive wave speeds and at a current grid point for the negative wave speed. In contrast, a standard wave-splitting scheme typically employs a half-point method such as

$$\mathbf{A}_{i-\frac{1}{2}}^{+} = \mathbf{A}^{+}\left(\frac{\mathbf{y}_{i-1}+\mathbf{y}_i}{2}, \frac{x_{i-1}+x_i}{2}\right) \tag{48}$$

$$\mathbf{A}_{i+\frac{1}{2}}^{-} = \mathbf{A}^{-}\left(\frac{\mathbf{y}_i+\mathbf{y}_{i+1}}{2}, \frac{x_i+x_{i+1}}{2}\right) \tag{49}$$

B. Stability Analysis

In the presence of the non-homogeneous source vector $\mathbf{B}$, the stability of the upwind finite difference method could be impacted depending upon the magnitude of $\mathbf{B}$. Global stability of nonlinear differential equations is very desirable, but in many cases it can be difficult to evaluate. Lyapunov stability theory has been used for determining global stability of nonlinear differential equations. Nonetheless, finding a Lyapunov function for a nonlinear system can be quite daunting and the failure of finding one does not necessarily imply that the system is unstable. Most often,

local stability of a nonlinear differential equation can be inferred from global stability of the linearization about an equilibrium. Suppose $\mathbf{y}_i$ is the steady state solution of Eq. (38), then for every $\mathbf{y}_i \in \mathbb{R}^n$ there exists a small variation $\widetilde{\mathbf{y}}_i$ around the neighborhood of $\mathbf{y}_i$ such that if $\widetilde{\mathbf{y}}_i$ is bounded throughout the neighborhood of $\mathbf{y}_i$, then $\widetilde{\mathbf{y}}_i$ is globally stable. Global stability of $\widetilde{\mathbf{y}}_i$ implies local stability of $\mathbf{y}_i$.

Suppose $\mathbf{A}^+_{i-1}$, $\mathbf{A}^-_i$, $\mathbf{B}^+_{i-1}$, and $\mathbf{B}^-_i$ are locally Lipschitz with respect to $\mathbf{y}_{i-1}$ and $\mathbf{y}_i$, then to obtain $\widetilde{\mathbf{y}}_i$, we linearize Eq. (42) as

$$\begin{aligned}\dot{\widetilde{\mathbf{y}}}_i + \mathbf{A}^+_{i-1}\frac{\widetilde{\mathbf{y}}_i - \widetilde{\mathbf{y}}_{i-1}}{\Delta x} + \mathbf{A}^+_{i-1,\mathbf{y}_i}\left(\frac{\mathbf{y}_i - \mathbf{y}_{i-1}}{\Delta x}\right)\widetilde{\mathbf{y}}_i + \mathbf{A}^+_{i-1,\mathbf{y}_{i-1}}\left(\frac{\mathbf{y}_i - \mathbf{y}_{i-1}}{\Delta x}\right)\widetilde{\mathbf{y}}_{i-1} \\ + \mathbf{A}^-_i\frac{\widetilde{\mathbf{y}}_{i+1} - \widetilde{\mathbf{y}}_i}{\Delta x} + \mathbf{A}^-_{i,\mathbf{y}_i}\left(\frac{\mathbf{y}_{i+1} - \mathbf{y}_i}{\Delta x}\right)\widetilde{\mathbf{y}}_i + \mathbf{A}^-_{i,\mathbf{y}_{i-1}}\left(\frac{\mathbf{y}_{i+1} - \mathbf{y}_i}{\Delta x}\right)\widetilde{\mathbf{y}}_{i-1} \\ + \left(\mathbf{B}^+_{i-1,\mathbf{y}_i} + \mathbf{B}^-_{i,\mathbf{y}_i}\right)\widetilde{\mathbf{y}}_i + \left(\mathbf{B}^+_{i-1,\mathbf{y}_{i-1}} + \mathbf{B}^-_{i,\mathbf{y}_{i-1}}\right)\widetilde{\mathbf{y}}_{i-1} = \mathbf{0}\end{aligned} \tag{50}$$

Since $\mathbf{y}_i$ is a steady state solution, then it follows that

$$\frac{\mathbf{y}_{i+1} - \mathbf{y}_i}{\Delta x} = -\mathbf{C}_i \tag{51}$$

where $\mathbf{C}_i = \mathbf{A}^{-1}\left(\mathbf{Y}_i, x_i\right)\mathbf{B}\left(\mathbf{Y}_i, x_i\right)$ as defined in Eq. (23). Equation (50) then becomes

$$\begin{aligned}\dot{\widetilde{\mathbf{y}}}_i + \mathbf{A}^+_{i-1}\frac{\widetilde{\mathbf{y}}_i - \widetilde{\mathbf{y}}_{i-1}}{\Delta x} + \mathbf{A}^-_i\frac{\widetilde{\mathbf{y}}_{i+1} - \widetilde{\mathbf{y}}_i}{\Delta x} + \left(\mathbf{B}^+_{i-1,\mathbf{y}_i} + \mathbf{B}^-_{i,\mathbf{y}_i} - \mathbf{A}^+_{i-1,\mathbf{y}_i}\mathbf{C}_{i-1} - \mathbf{A}^-_{i,\mathbf{y}_i}\mathbf{C}_i\right)\widetilde{\mathbf{y}}_i \\ + \left(\mathbf{B}^+_{i-1,\mathbf{y}_{i-1}} + \mathbf{B}^-_{i,\mathbf{y}_{i-1}} - \mathbf{A}^+_{i-1,\mathbf{y}_{i-1}}\mathbf{C}_{i-1} - \mathbf{A}^-_{i,\mathbf{y}_{i-1}}\mathbf{C}_i\right)\widetilde{\mathbf{y}}_{i-1} = \mathbf{0}\end{aligned} \tag{52}$$

The term $\mathbf{A}^+_{i-1,\mathbf{y}_i}\mathbf{C}_{i-1}$ is evaluated at $\mathbf{y}_{i-1}$ and $\mathbf{y}_i$ as

$$\mathbf{A}^+_{i-1,\mathbf{y}_i}\mathbf{C}_{i-1} = \left[\begin{array}{ccc} \mathbf{A}^+_{i-1,y_{1,i}}\mathbf{C}_{i-1} & \mathbf{A}^+_{i-1,y_{2,i}}\mathbf{C}_{i-1} & \mathbf{A}^+_{i-1,y_{3,i}}\mathbf{C}_{i-1} \end{array}\right]_{3\times 3} \tag{53}$$

where the subscript y_j, $j = 1, 2, 3$ denotes the partial derivative with respect to the scalar quantity y_j. All the other terms $\mathbf{A}^-_{i,\mathbf{y}_i}\mathbf{C}_i$, $\mathbf{A}^+_{i-1,\mathbf{y}_{i-1}}\mathbf{C}_{i-1}$, and $\mathbf{A}^-_{i,\mathbf{y}_{i-1}}\mathbf{C}_i$ in Eq. (52) are then evaluated in the same manner.

If $\mathbf{y}_i$ is smooth and Δx is a small number, then it may be assumed that $\mathbf{A}^-_i \simeq \mathbf{A}^-_{i-1}$, $\mathbf{A}_{i-1,\mathbf{y}_i}\mathbf{C}_{i-1} \simeq \mathbf{A}^+_{i-1,\mathbf{y}_i}\mathbf{C}_{i-1} + \mathbf{A}^-_{i,\mathbf{y}_i}\mathbf{C}_i$, and $\mathbf{B}_{i-1,\mathbf{y}_i} \simeq \mathbf{B}^+_{i-1,\mathbf{y}_i} + \mathbf{B}^-_{i,\mathbf{y}_i}$. Furthermore, we recognize that

$$\mathbf{A}^{-1}_{i-1}\mathbf{A}_{i-1,\mathbf{y}_i}\mathbf{C}_{i-1} + \mathbf{A}^{-1}_{i-1,\mathbf{y}_i}\mathbf{A}_{i-1}\mathbf{C}_{i-1} = 0 \Rightarrow \mathbf{A}_{i-1,\mathbf{y}_i}\mathbf{C}_{i-1} = -\mathbf{A}_{i-1}\mathbf{A}^{-1}_{i-1,\mathbf{y}_i}\mathbf{B}_{i-1} \tag{54}$$

Then, it follows that

$$\mathbf{B}_{i-1,\mathbf{y}_i} - \mathbf{A}_{i-1,\mathbf{y}_i}\mathbf{C}_{i-1} = \mathbf{A}_{i-1}\left(\mathbf{A}^{-1}_{i-1}\mathbf{B}_{i-1,\mathbf{y}_i} + \mathbf{A}^{-1}_{i-1,\mathbf{y}_i}\mathbf{B}_{i-1}\right) = \mathbf{A}_{i-1}\mathbf{C}_{i-1,\mathbf{y}_i} \tag{55}$$

We now can simplify Eq. (52) as

$$\dot{\widetilde{\mathbf{y}}}_i + \mathbf{A}^+_{i-1}\frac{\widetilde{\mathbf{y}}_i - \widetilde{\mathbf{y}}_{i-1}}{\Delta x} + \mathbf{A}^-_{i-1}\frac{\widetilde{\mathbf{y}}_{i+1} - \widetilde{\mathbf{y}}_i}{\Delta x} + \mathbf{A}_{i-1}\mathbf{C}_{i-1,\mathbf{y}_i}\widetilde{\mathbf{y}}_i + \mathbf{A}_{i-1}\mathbf{C}_{i-1,\mathbf{y}_{i-1}}\widetilde{\mathbf{y}}_{i-1} \simeq \mathbf{0} \tag{56}$$

where

$$\mathbf{C}_{\mathbf{y}} = \frac{kp_0M^2}{1-M^2}\left[\begin{array}{ccc} 0 & 0 & 0 \\ \frac{1}{\dot{m}}\left(\frac{T_0 f}{TD} + \frac{1+kM^2}{2\dot{m}c_pT_0}\frac{dQ}{dx}\right) & -\frac{1+kM^2}{2p_0}\left(\frac{f}{D} + \frac{1}{\dot{m}c_pT_0}\frac{d\bar{Q}}{dx}\right) & \frac{1}{2T_0}\left(\frac{T_0 f}{TD} + \frac{(k+1)M^2}{2\dot{m}c_pT_0}\frac{dQ}{dx}\right) \\ \frac{1-M^2}{kp_0M^2\dot{m}^2c_p}\frac{dQ}{dx} & 0 & 0 \end{array}\right] \tag{57}$$

Equation (56) can be written in a form

$$\dot{\mathbf{X}} = \mathbf{S}\mathbf{X} + \mathbf{V} \tag{58}$$

where $\mathbf{X} = \begin{bmatrix} \widetilde{\mathbf{y}}_2 & \widetilde{\mathbf{y}}_3 & \cdots & \widetilde{\mathbf{y}}_{m-1} \end{bmatrix}^T$, $\mathbf{V} = \begin{bmatrix} \left(\frac{\mathbf{A}_1^+}{\Delta x} - \mathbf{A}_1\mathbf{C}_{1,\mathbf{y}_1}\right)\widetilde{\mathbf{y}}_1 & \mathbf{0} & \cdots & -\frac{\mathbf{A}_{m-2}^-}{\Delta x}\ \widetilde{\mathbf{y}}_m \end{bmatrix}^T$,

$$\mathbf{S} = \begin{bmatrix} -\frac{|\mathbf{A}_1|}{\Delta x} - \mathbf{A}_1\mathbf{C}_{1,\mathbf{y}_2} & -\frac{\mathbf{A}_1^-}{\Delta x} & \cdots & \mathbf{0} \\ \frac{\mathbf{A}_2^+}{\Delta x} - \mathbf{A}_2\mathbf{C}_{2,\mathbf{y}_2} & -\frac{|\mathbf{A}_2|}{\Delta x} - \mathbf{A}_2\mathbf{C}_{2,\mathbf{y}_3} & -\frac{\mathbf{A}_2^-}{\Delta x} & \vdots \\ \vdots & \mathbf{0} & \ddots & -\frac{\mathbf{A}_{m-3}^-}{\Delta x} \\ \mathbf{0} & \cdots & \frac{\mathbf{A}_{m-2}^+}{\Delta x} - \mathbf{A}_{m-2}\mathbf{C}_{m-2,\mathbf{y}_{m-2}} & -\frac{|\mathbf{A}_{m-2}|}{\Delta x} - \mathbf{A}_{m-2}\mathbf{C}_{m-2,\mathbf{y}_{m-1}} \end{bmatrix} \tag{59}$$

and $|\mathbf{A}_i| = \mathbf{A}_i^+ - \mathbf{A}_i^-$.

For a homogeneous solution for which $\mathbf{Z} = \mathbf{0}$, Eq. (58) is stable if the eigenvalues of $\mathbf{S}$ are negative, thereby implying that Eq. (42) is locally stable about its equilibrium. The effect of the non-homogeneous term $\mathbf{Z}$ on the stability will be discussed later. If $\mathbf{y}_i$ is smooth and Δx is small, then the eigenvalues of $\mathbf{S}$ are computed to be

$$\lambda(\mathbf{S}) = \lambda\left(-\frac{|\mathbf{A}_i|}{\Delta x} - \mathbf{A}_i\mathbf{C}_{i,\mathbf{y}_i} \pm \left[-\frac{\mathbf{A}_i^-}{\Delta x}\left(\frac{\mathbf{A}_i^+}{\Delta x} - \mathbf{A}_i\mathbf{C}_{i,\mathbf{y}_i}\right)\right]^{\frac{1}{2}}\right) \tag{60}$$

where $\lambda(*)$ denotes the eigenvalue operation on * and the square root operation of the matrix can be computed using a singular value decomposition.

Using the fact that $\mathbf{A}_i^-\mathbf{A}_i^+ = \mathbf{0}$ and $\mathbf{A}_i^-\mathbf{A}_i = \mathbf{A}_i^-\mathbf{A}_i^-$, then Eq. (60) can be simplified as

$$\lambda(\mathbf{S}) = \lambda\left(-\mathbf{A}_i^+\left(\frac{\mathbf{I}}{\Delta x} + \mathbf{C}_{i,\mathbf{y}_i}\right) + \mathbf{A}_i^-\left[\frac{\mathbf{I}}{\Delta x} - \mathbf{C}_{i,\mathbf{y}_i} \pm \left(\frac{\mathbf{C}_{i,\mathbf{y}_i}}{\Delta x}\right)^{\frac{1}{2}}\right]\right) \tag{61}$$

For stability, we require that $\lambda(\mathbf{S}) < 0$. Since $\mathbf{A}_i^+ \geq \mathbf{0}$ and $\mathbf{A}_i^- \leq \mathbf{0}$, this implies that

$$\frac{\mathbf{I}}{\Delta x} + \mathbf{C}_{i,\mathbf{y}_i} > \mathbf{0} \tag{62}$$

$$\frac{\mathbf{I}}{\Delta x} - \mathbf{C}_{i,\mathbf{y}_i} \pm \left(\frac{\mathbf{C}_{i,\mathbf{y}_i}}{\Delta x}\right)^{\frac{1}{2}} > \mathbf{0} \tag{63}$$

where $\mathbf{I}$ is the identity matrix. Since $\lambda(\mathbf{C}_\mathbf{y}) \leq \mathbf{0}$, this implies that $\mathbf{C}_{i,\mathbf{y}_i} \leq \mathbf{0}$. Eq. (63) then has an imaginary part, so we only require that the real part be positive definite. Because $\mathbf{C}_{i,\mathbf{y}_i} \leq \mathbf{0}$, Eq. (63) is satisfied for all Δx. On the other hand, Eq. (62) places a restriction on Δx which must satisfy

$$\Delta x < \frac{1}{\max|\lambda(\mathbf{C}_{i,\mathbf{y}_i})|} \tag{64}$$

where

$$\max|\lambda(\mathbf{C}_\mathbf{y})| = \frac{kM^2\left(1+kM^2\right)}{1-M^2}\left(\frac{f}{D} + \frac{1}{\dot{m}c_pT_0}\frac{d\bar{Q}}{dx}\right) \tag{65}$$

We see that the presence of the non-homogeneous source term $\mathbf{B}$ in Eq. (4) affects the stability of the wave-splitting scheme in Eq. (42) which requires that Δx be less than the reciprocal of the largest absolute eigenvalue of $\mathbf{C}_{i,\mathbf{y}}$. Thus far, we have not considered the effect of the non-homogeneous term $\mathbf{Z}$. It is obvious that the stability of Eq. (58) also requires that $\mathbf{Z}$ is bounded in $t \in [0, T]$. We assume that the functions $\mathbf{g}(\mathbf{y}(L,t), \mathbf{u})$ and $\mathbf{f}$ are locally Lipschitz with respect to $\mathbf{y}_1(t) = \mathbf{y}(0,t)$, $\mathbf{y}_m(t) = \mathbf{y}(L,t)$, and $\mathbf{u}$. If $\mathbf{u} \in \mathbb{R}^m$ is the steady state solution of Eq. (27), then there exists a small variation $\widetilde{\mathbf{u}}$ around the neighborhood of $\mathbf{u}$ such that if $\widetilde{\mathbf{u}}$ is bounded throughout the neighborhood of $\mathbf{u}$, then $\widetilde{\mathbf{u}}$ is globally stable. Linearization of Eqs. (25) and (27) result in

$$\mathbf{V} = \begin{bmatrix} \left(\frac{\mathbf{A}_1^+}{\Delta x} - \mathbf{A}_1\mathbf{C}_{1,\mathbf{y}_1}\right)\left(\mathbf{g}_{\mathbf{y}_m}\widetilde{\mathbf{y}}_m + \mathbf{g}_\mathbf{u}\widetilde{\mathbf{u}}\right) & \mathbf{0} & \cdots & -\frac{\mathbf{A}_{m-1}^-}{\Delta x}\ \widetilde{\mathbf{y}}_m \end{bmatrix}^T \tag{66}$$

$$\dot{\widetilde{\mathbf{u}}} = \mathbf{f}_\mathbf{u}\widetilde{\mathbf{u}} + \mathbf{f}_{\mathbf{y}_1}\widetilde{\mathbf{y}}_1 + \mathbf{f}_{\mathbf{y}_m}\widetilde{\mathbf{y}}_m + \mathbf{f}_\mathbf{V}\widetilde{\mathbf{v}} \tag{67}$$

The non-homogeneous term $\mathbf{Z}$ is bounded if Eq. (67) is globally stable. Since $\mathbf{V}$ is measurable in L^2, then $\widetilde{\mathbf{v}}$ is also measurable in L^2. The local stability of Eq. (27) then requires the global stability of Eq. (67) which implies that the eigenvalues of $\mathbf{f_u}$ are negative in order to ensure that the non-homogeneous term $\mathbf{Z}$ is always bounded in $t \in [0, T]$. Thus, the additional requirement for the wave-splitting scheme is

$$\lambda\left(\mathbf{f_u}\right) < 0 \tag{68}$$

We have thus shown that the wave-splitting scheme in Eq. (42) is stable under certain requirements. To implement the complete computational procedure, we must also address the nonlinear dynamic constraint equation (27) which can be discretized as

$$\dot{\mathbf{u}} = \mathbf{f}\left(\mathbf{y}_1, \mathbf{y}_m, \mathbf{u}, \mathbf{V}\right) \tag{69}$$

Equations (42) and (69) are subject to the following initial conditions

$$\mathbf{y}_i\left(0\right) = \mathbf{h}\left(x_i\right) \tag{70}$$

$$\mathbf{u}\left(0\right) = \mathbf{u}_0 \tag{71}$$

Both these equations can be integrated using any standard ODE numerical methods such as the Euler's method or the Runge-Kutta method. We note that because of the nonlinear forced periodic boundary condition (25) and the quasi-linearity of Eq. (4), Eqs. (42) and (69) must be discretized in time using an explicit scheme. For an Euler's method, the time step must be chosen to satisfy the following condition

$$\Delta t \leq \min\left\{\frac{\Delta x}{\max\left[\left(1+\alpha_i\right)\left(u_i+c_i\right)\right]}, \frac{2}{\max\left|\lambda\left(\mathbf{f_u}\right)\right|}\right\} \tag{72}$$

The first condition is the Courant-Friedrichs-Levy (CFL) condition for Eq. (42). The term $1+\alpha$ is due to the contribution of the source term $\mathbf{C}$. The second condition is the numerical stability condition for the Euler's method for Eq. (69).

C. Boundary Condition and Characteristic Equations

To solve for Eq. (39), we need the information on the system boundaries. We can write the periodic boundary condition (25) in a component form as

$$\begin{bmatrix} \dot{m}\left(0,t\right) \\ p_0\left(0,t\right) \\ T_0\left(0,t\right) \end{bmatrix} = \begin{bmatrix} \mathbf{I}_1 \\ \mathbf{I}_2 \\ \mathbf{I}_3 \end{bmatrix} \mathbf{y}_{1,j+1} = \begin{bmatrix} g_1\left(\mathbf{y}_{m,j+1}, \mathbf{u}_{j+1}\right) \\ g_2\left(\mathbf{y}_{m,j+1}, \mathbf{u}_{j+1}\right) \\ g_3\left(\mathbf{y}_{m,j+1}, \mathbf{u}_{j+1}\right) \end{bmatrix} \tag{73}$$

where $\mathbf{I}_k$, $k = 1, 2, 3$, is a k-th row vector of the 3×3 identity matrix, and $j = 1, 2, \ldots, n-1$ denotes the time index such that $t_j = \frac{j-1}{n-1}T$ and $\mathbf{y}_{ij} = \mathbf{y}\left(x_i, t_j\right)$. We note that the mass flow is generally conserved so that

$$g_1\left(\mathbf{y}_{m,j+1}, \mathbf{u}_{j+1}\right) = \mathbf{I}_1 \mathbf{y}_{m,j+1} \tag{74}$$

At the incoming boundary $x = 0$, $i = 1$ so that the Eq. (37) cannot admit a positive wave which would require the solution to include a point upstream of $x = 0$ that is nonexistent. Since there is only one negative wave, only the negative wave speed characteristic equation (41) is admitted. Using the Euler's method, we combine Eq. (41) with the last two components of the boundary condition (73) so that

$$\begin{bmatrix} \mathbf{I}_2 \\ \mathbf{I}_3 \\ \mathbf{\Psi}_3\left(\mathbf{y}_{1j}, x_1\right) \end{bmatrix} \mathbf{y}_{1,j+1} - \begin{bmatrix} g_2\left(\mathbf{y}_{m,j+1}, \mathbf{u}_{j+1}\right) \\ g_3\left(\mathbf{y}_{m,j+1}, \mathbf{u}_{j+1}\right) \\ 0 \end{bmatrix} = \begin{bmatrix} \mathbf{0}_{1\times 3} \\ \mathbf{0}_{1\times 3} \\ \mathbf{\Psi}_3\left(\mathbf{y}_{1j}, x_1\right) \end{bmatrix} \mathbf{y}_{1j}$$
$$- \frac{\mathbf{\Lambda}^-\left(\mathbf{y}_{1j}, x_1\right)\Delta t}{\Delta x} \begin{bmatrix} \mathbf{0}_{1\times 3} \\ \mathbf{0}_{1\times 3} \\ \mathbf{\Psi}_3\left(\mathbf{y}_{1j}, x_1\right) \end{bmatrix} \left(\mathbf{y}_{2j} - \mathbf{y}_{1j}\right) - \begin{bmatrix} \mathbf{0}_{1\times 3} \\ \mathbf{0}_{1\times 3} \\ \mathbf{\Psi}_3\left(\mathbf{y}_{1j}, x_1\right) \end{bmatrix} \Delta t \mathbf{B}\left(\mathbf{y}_{1j}, x_1\right) \tag{75}$$

where $\mathbf{0}_{1\times 3}$ is the 1×3 zero row vector.

We next consider the boundary at $x = L$, $i = m$. The situation is now reverse whereby the solution can only admit the two positive eigenvalue characteristic equations (39) and (40) along with the first component of the boundary condition (73). These three equations are written in a matrix form as

$$\begin{aligned}\begin{bmatrix} \boldsymbol{\Psi}_1\left(\mathbf{y}_{m-1,j}, x_{m-1}\right) \\ \boldsymbol{\Psi}_2\left(\mathbf{y}_{m-1,j}, x_{m-1}\right) \\ \mathbf{I}_1 \end{bmatrix} \mathbf{y}_{m,j+1} - \begin{bmatrix} \mathbf{0}_{1\times 3} \\ \mathbf{0}_{1\times 3} \\ \mathbf{I}_1 \end{bmatrix} \mathbf{y}_{1,j+1} = \begin{bmatrix} \boldsymbol{\Psi}_1\left(\mathbf{y}_{m-1,j}, x_{m-1}\right) \\ \boldsymbol{\Psi}_2\left(\mathbf{y}_{m-1,j}, x_{m-1}\right) \\ \mathbf{0}_{1\times 3} \end{bmatrix} \mathbf{y}_{mj} \\ - \frac{\boldsymbol{\Lambda}^+\left(\mathbf{y}_{m-1,j}, x_{m-1}\right)\Delta t}{\Delta x} \begin{bmatrix} \boldsymbol{\Psi}_1\left(\mathbf{y}_{m-1,j}, x_{m-1}\right) \\ \boldsymbol{\Psi}_2\left(\mathbf{y}_{m-1,j}, x_{m-1}\right) \\ \mathbf{0}_{1\times 3} \end{bmatrix} \left(\mathbf{y}_{mj} - \mathbf{y}_{m-1,j}\right) \\ - \begin{bmatrix} \boldsymbol{\Psi}_1\left(\mathbf{y}_{m-1,j}, x_{m-1}\right) \\ \boldsymbol{\Psi}_2\left(\mathbf{y}_{m-1,j}, x_{m-1}\right) \\ \mathbf{0}_{1\times 3} \end{bmatrix} \Delta t \mathbf{B}\left(\mathbf{y}_{m-1,j}, x_{m-1}\right) \end{aligned} \tag{76}$$

Equations (75) and (76) are nonlinear at the time step t_{j+1} due to the boundary condition (73) and also coupled together through the term $\mathbf{y}_{1,j+1}$. Solving for $\mathbf{y}_{1,j+1}$ from Eq. (75) and substituting into Eq. (76) then yield

$$\begin{aligned}&\begin{bmatrix} \boldsymbol{\Psi}_1\left(\mathbf{y}_{m-1,j}, x_{m-1}\right) \\ \boldsymbol{\Psi}_2\left(\mathbf{y}_{m-1,j}, x_{m-1}\right) \\ \mathbf{I}_1 \end{bmatrix} \mathbf{y}_{m,j+1} - \begin{bmatrix} \mathbf{0}_{1\times 3} \\ \mathbf{0}_{1\times 3} \\ \mathbf{I}_1 \end{bmatrix} \begin{bmatrix} \mathbf{I}_2 \\ \mathbf{I}_3 \\ \boldsymbol{\Psi}_3\left(\mathbf{y}_{1j}, x_1\right) \end{bmatrix}^{-1} \begin{bmatrix} g_2\left(\mathbf{y}_{m,j+1}, \mathbf{u}_{j+1}\right) \\ g_3\left(\mathbf{y}_{m,j+1}, \mathbf{u}_{j+1}\right) \\ \mathbf{0}_{1\times 3} \end{bmatrix} = \\ &\begin{bmatrix} \boldsymbol{\Psi}_1\left(\mathbf{y}_{m-1,j}, x_{m-1}\right) \\ \boldsymbol{\Psi}_2\left(\mathbf{y}_{m-1,j}, x_{m-1}\right) \\ \mathbf{0}_{1\times 3} \end{bmatrix} \mathbf{y}_{mj} - \frac{\boldsymbol{\Lambda}^+\left(\mathbf{y}_{m-1j}, x_{m-1}\right)\Delta t}{\Delta x} \begin{bmatrix} \boldsymbol{\Psi}_1\left(\mathbf{y}_{m-1,j}, x_{m-1}\right) \\ \boldsymbol{\Psi}_2\left(\mathbf{y}_{m-1,j}, x_{m-1}\right) \\ \mathbf{0}_{1\times 3} \end{bmatrix} \left(\mathbf{y}_{mj} - \mathbf{y}_{m-1,j}\right) \\ &- \begin{bmatrix} \boldsymbol{\Psi}_1\left(\mathbf{y}_{m-1,j}, x_{m-1}\right) \\ \boldsymbol{\Psi}_2\left(\mathbf{y}_{m-1,j}, x_{m-1}\right) \\ \mathbf{0}_{1\times 3} \end{bmatrix} \Delta t \mathbf{B}\left(\mathbf{y}_{m-1,j}, x_{m-1}\right) + \begin{bmatrix} \mathbf{0}_{1\times 3} \\ \mathbf{0}_{1\times 3} \\ \mathbf{I}_1 \end{bmatrix} \begin{bmatrix} \mathbf{I}_2 \\ \mathbf{I}_3 \\ \boldsymbol{\Psi}_3\left(\mathbf{y}_{1j}, x_1\right) \end{bmatrix}^{-1} \begin{bmatrix} \mathbf{0}_{1\times 3} \\ \mathbf{0}_{1\times 3} \\ \boldsymbol{\Psi}_3\left(\mathbf{y}_{1j}, x_1\right) \end{bmatrix} \mathbf{y}_{1j} \\ &- \begin{bmatrix} \mathbf{0}_{1\times 3} \\ \mathbf{0}_{1\times 3} \\ \mathbf{I}_1 \end{bmatrix} \begin{bmatrix} \mathbf{I}_2 \\ \mathbf{I}_3 \\ \boldsymbol{\Psi}_3\left(\mathbf{y}_{1j}, x_1\right) \end{bmatrix}^{-1} \frac{\boldsymbol{\Lambda}^-\left(\mathbf{y}_{1j}, x_1\right)\Delta t}{\Delta x} \begin{bmatrix} \mathbf{0}_{1\times 3} \\ \mathbf{0}_{1\times 3} \\ \boldsymbol{\Psi}_3\left(\mathbf{y}_{1j}, x_1\right) \end{bmatrix} \left(\mathbf{y}_{2j} - \mathbf{y}_{1j}\right) \\ &- \begin{bmatrix} \mathbf{0}_{1\times 3} \\ \mathbf{0}_{1\times 3} \\ \mathbf{I}_1 \end{bmatrix} \begin{bmatrix} \mathbf{I}_2 \\ \mathbf{I}_3 \\ \boldsymbol{\Psi}_3\left(\mathbf{y}_{1j}, x_1\right) \end{bmatrix}^{-1} \begin{bmatrix} \mathbf{0}_{1\times 3} \\ \mathbf{0}_{1\times 3} \\ \boldsymbol{\Psi}_3\left(\mathbf{y}_{1j}, x_1\right) \end{bmatrix} \Delta t \mathbf{B}\left(\mathbf{y}_{1j}, x_1\right) \end{aligned} \tag{77}$$

Equation (77) now becomes only a nonlinear function of $\mathbf{y}_{m,j+1}$ and $\mathbf{u}_{j+1}$. An iterative method is implemented to search for the zero solution of $\mathbf{y}_{m,j+1}$ using information from the previous time step. To solve Eq. (77), the boundary control vector $\mathbf{u}$ must be determined for a given time history of the auxiliary control $\mathbf{V}$ by integrating Eq. (69). Once $\mathbf{y}_{m,j+1}$ is determined, then $\mathbf{y}_{m,j+1}$ is computed from Eq. (76). Thus, the information at the system boundaries is now known and then can be used to compute all the information at the interior points by integrating Eq. (42) forward in time.

D. Shock Capturing

Flow with shocks in a closed-loop transport systems pose a significant challenge in that a discontinuous solution of the Euler equations must be found that can predict when and where a shock structure would arise. To further complicate the solution, the discontinuous solution must also satisfy the nonlinear boundary condition (25). Most shock capturing schemes are designed for the conservation form of the Euler equations because the flux variables are conserved across a shock structure. First-order shock capturing schemes such as Lax-Friedrichs and Lax-Wendroff schemes with artificial viscosity are commonly used to provide unique entropy solutions that define physical shock structures.

Herein, we present a shock capturing method for the non-conservation form of the Euler equations. Toward that end, if the flow in a closed-loop transport system is transitioned from subsonic to supersonic, the critical flow condition at Mach 1 exists at the minimum cross sectional area A^*, or the throat area. The ensuing supersonic flow will encounter a normal shock formation at some point farther downstream in the flow from the throat area. In this situation, the flow in the closed-loop transport system can be divided into three regions: 1) region I is defined by $0 \leq x < L^*$ wherein the flow is entirely subsonic, 2) region II is defined by $L^* < x \leq L_S^-$ wherein the flow is entirely supersonic, and 3) region III is defined by $L_S^- < x \leq L$ wherein the flow is entirely subsonic. The discontinuous solution across the shock region $L_S^- < x \leq L_S^+$ is defined by the Rankine-Hugoniot relationship

$$\left(\mathbf{F}^+ - \mathbf{F}^-\right) = V\left(\mathbf{U}^+ - \mathbf{U}^-\right) \tag{78}$$

which can also be written as

$$\left(\mathbf{b}^+\mathbf{y}^+ - \mathbf{b}^-\mathbf{y}^-\right) = V\left(\mathbf{a}^+\mathbf{y}^+ - \mathbf{a}^-\mathbf{y}^-\right) \tag{79}$$

where the $\pm$ sign denotes $x = L_S^+$ and $x = L_S^-$, V is the speed of the moving shock, and

$$\mathbf{a}\left(\mathbf{y}\right) = \begin{bmatrix} \frac{1}{u} & 0 & 0 \\ 1 & 0 & 0 \\ 0 & -\frac{A}{\left(1+\frac{\gamma-1}{2}M^2\right)^{\frac{\gamma}{\gamma-1}}} & \frac{\dot{m}c_p}{u} \end{bmatrix} \quad \mathbf{b}\left(\mathbf{y}, x\right) = \begin{bmatrix} 1 & 0 & 0 \\ 0 & \frac{A\left(1+\gamma M^2\right)}{\left(1+\frac{\gamma-1}{2}M^2\right)^{\frac{\gamma}{\gamma-1}}} & 0 \\ 0 & 0 & \dot{m}c_p \end{bmatrix} \tag{80}$$

To obtain a physical solution, the entropy condition requires that

$$M^+ - \frac{V}{c^+} = \sqrt{\frac{2 + (\gamma-1)\left(M^- - \frac{V}{c^-}\right)^2}{2\gamma\left(M^- - \frac{V}{c^-}\right)^2 - (\gamma-1)}} < 1 \tag{81}$$

We note that for a standing shock, the following relationship applies

$$\mathbf{y}^+ = \left(\mathbf{b}^+\right)^{-1}\mathbf{b}^-\mathbf{y}^- \tag{82}$$

where

$$\left(\mathbf{b}^+\right)^{-1}\mathbf{b}^- = \begin{bmatrix} 1 & 0 & 0 \\ 0 & r & 0 \\ 0 & 0 & 1 \end{bmatrix} \tag{83}$$

$$r = \left[\frac{\frac{\gamma+1}{2}\left(M^-\right)^2}{1 + \frac{\gamma+1}{2}\left(M^-\right)^2}\right]^{\frac{\gamma}{\gamma-1}} \left[\frac{2\gamma}{\gamma+1}\left(M^-\right)^2 - \frac{\gamma-1}{\gamma+1}\right]^{-\frac{1}{\gamma-1}} < 1 \tag{84}$$

The shock location L_S is determined by matching the flow conditions at the boundaries between the flow regions in order to satisfy the nonlinear forced periodic boundary condition (25). Initially, we assume a standing shock whose location is known. At each subsequent time step, an iterative solution is performed to locate the shock. Since the mass flow and enthalpy conservation prevails at the boundaries of these regions, the shock location is primarily a function of the stagnation pressure relationship and is found by determining $x = L_S$ that satisfies the following stagnation pressure balance equation

$$\Delta p_{0,I} + \Delta p_{0,II} + \Delta p_{0,S} + \Delta p_{0,III} = g_2\left(\mathbf{y}\left(L,t\right),\mathbf{u}\right) - p_0\left(L,t\right) \tag{85}$$

where

$$\Delta p_{0,I} = p_0\left(0,t\right) - p_0\left(L^*,t\right) \tag{86}$$

$$\Delta p_{0,II} = p_0\left(L^*,t\right) - p_0\left(L_S^-,t\right) \tag{87}$$

$$\Delta p_{0,S} = p_0\left(L_S^-,t\right) - p_0\left(L_S^+,t\right) = -\frac{V}{b_{22}^+}\left(\dot{m}^+ - \dot{m}^-\right) + \left(1 - \frac{b_{22}^-}{b_{22}^+}\right)p_0^- \tag{88}$$

$$\Delta p_{0,III} = p_0\left(L_S^+,t\right) - p_0\left(L,t\right) \tag{89}$$

To solve for flow regions I and II, an additional boundary condition is imposed at the throat area that relates the critical mass flow to the stagnation pressure and temperature as follows:

$$\dot{m}\left(L^*,t\right)=\sqrt{\frac{\gamma}{RT_0\left(L^*,t\right)}}p_0\left(L^*,t\right)A^*\left(\frac{\gamma+1}{2}\right)^{-\frac{\gamma+1}{2(\gamma-1)}} \tag{90}$$

This boundary condition together with two characteristic boundary conditions for positive wave speeds completely define the boundary conditions at the throat area. Once the initial guess of the shock location at the current time step is found, the normal shock speed can be computed from the shock locations at the current and previous time steps as

$$V=\frac{L_S\left(t\right)-L_S\left(t-\Delta t\right)}{\Delta t} \tag{91}$$

Equations (79), (85), and (91) are then iterated until the shock location L_S converges. The solution for the entire transonic flow in the closed-loop transport system is then completely established.

IV. Numerical Simulation

A. Closed-Circuit Wind Tunnel Model

The present computational method for a closed-loop transport system is applied to model fluid flow in a closed-circuit wind tunnel. Fig. 2 illustrates the NASA Ames 11-Foot Transonic Wind Tunnel (11-Ft TWT). Fluid flow is recirculated through a closed-circuit duct by a compressor that delivers air flow to a test section at a desired air speed for aerodynamic testing. The compressor is considered to be a key component of a wind tunnel system designed to match wind tunnel pressure losses due to fluid viscous losses. Fig. 3 illustrates a typical wind tunnel compressor. Fluid flow through alternating rows of stator and rotor blades within the compressor imparts a tangential velocity component in the flow. The kinetic energy associated with this swirl flow is then converted into a potential energy that creates a pressure rise across the compressor. The rotor blades are driven by a set of drive motors. In addition, a compressor in a wind tunnel may be equipped with variable-geometry inlet guide vanes designed to adjust the stagnation pressure rise at a constant compressor speed. The inlet guide vanes may have adjustable trailing edge flaps to change the air tangential velocity. Changes in the aerodynamic condition in a wind tunnel is thus accomplished by changing the compressor speed and the inlet guide vane flap angle. These two quantities are often referred to as compressor control inputs. Fig. 4 is a plot of the 11-Ft TWT Mach number envelope as a function of the compressor control inputs.

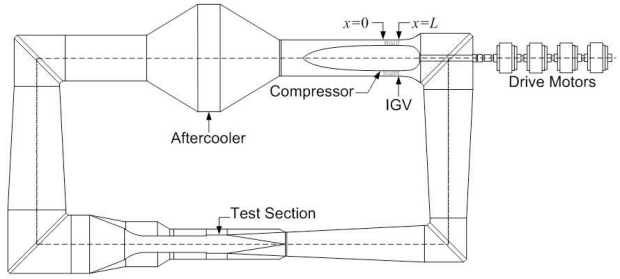

Fig. 2 - Closed-Circuit Wind Tunnel (NASA Ames 11-Ft TWT)

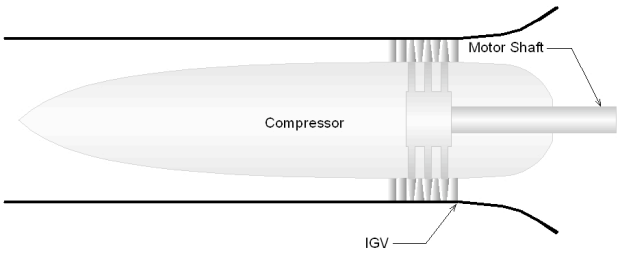

Fig. 3 - Wind Tunnel Compressor

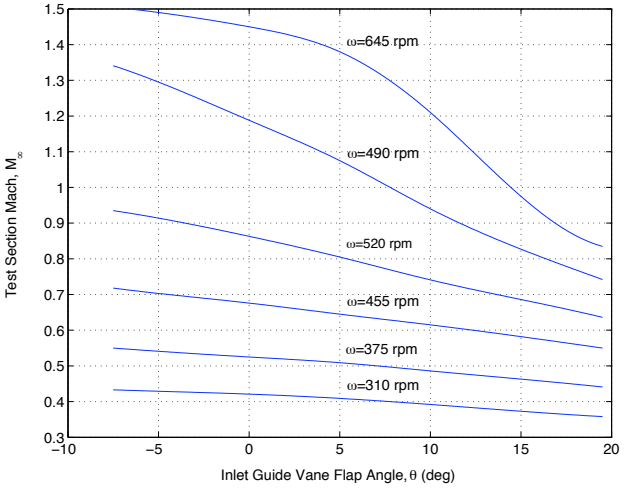

Fig. 4 - NASA Ames 11-Ft TWT Mach Number Envelope

The flow in a wind tunnel may be assumed to be 1-D flow since we are interested in unsteady, spatially averaged flow through any given cross section of the wind tunnel. This information is useful for studying the time response of the flow condition in the test section due to control inputs from the drive motors and the inlet guide vane flap angle. Equation (22) is used to model this 1-D unsteady flow. The friction factor f used in Eq. (22) is determined experimentally from wind tunnel measurements. The model also includes the heat transfer process taken place in the compressor and the aftercooler. We assume a perfect heat transfer process whereby the heat generated by the enthalpy increase across the compressor is completely removed by the aftercooler.

The forcing function $\mathbf{g}$ describes the behavior of the compressor through the boundary control vector $\mathbf{u} = \begin{bmatrix} \omega & \theta \end{bmatrix}^T$ where ω is the compressor speed and θ is the inlet guide vane flap angle. The compressor is a fluid device so the conservation of mass, momentum, and energy is applicable. The mass flow through the compressor must be constant. The stagnation pressure and stagnation temperature rises are due to the work input supplied by the drive motors. Let $x = 0$ be the compressor exit station and $x = L$ be the compressor inlet station. Then, the performance of a turbomachine is generally described by the following similitude relationship[11]

$$\frac{p_0(0,t)}{p_0(L,t)} = f(\dot{m}_c, \omega_c, \theta) \tag{92}$$

$$\frac{T_0(0,t)}{T_0(L,t)} = f\left(\frac{p_0(0,t)}{p_0(L,t)}, \dot{m}_c, \omega_c\right) \tag{93}$$

where $\dot{m}_c$ is the corrected mass flow and ω_c is the corrected speed defined as

$$\dot{m}_c = \dot{m}(L,t)\frac{p_{0,ref}}{p_0(L,t)}\sqrt{\frac{T_0(L,t)}{T_{0,ref}}} \tag{94}$$

$$\omega_c = \omega\sqrt{\frac{T_{0,ref}}{T_0(L,t)}} \tag{95}$$

and $p_{0,ref}$ and $T_{0,ref}$ are some reference total pressure and total temperature.

Using an empirical model, we obtain the forcing function $\mathbf{g}$ in the nonlinear forced periodic boundary condition (25) for the wind tunnel model as

$$\mathbf{g}(\mathbf{y}(L,t), \mathbf{u}) = \begin{bmatrix} \dot{m}(L,t) \\ p_0(L,t)\left(1 + \sum_{i=2}^{4}\sum_{j=0}^{2} c_{ij}\theta^j\omega_c^i\right)\left(b_1 - b_2\frac{\dot{m}_c}{\sum_{i=1}^{3}\sum_{j=0}^{2} d_{ij}\theta^j\omega_c^i}\right) \\ T_0(L,t)\left\{1 + \frac{b_3\omega_c}{\dot{m}_c}\left[\frac{p_0(0,t)}{p_0(L,t)} - 1\right]\right\} \end{bmatrix} \tag{96}$$

where b_i, c_{ij}, and d_{ij} are empirical coefficients derived from experimental compressor performance measurements as shown in Fig. 5.

Equation (27) describes the time-varying process of the boundary control as influenced by the dynamics of the auxiliary process encapsulated by the transition function $\mathbf{f}$ and the auxiliary control vector $\mathbf{V}$. The coupling with Eq. (22) is due to the existence of the transport vectors $\mathbf{y}(0,t)$ and $\mathbf{y}(L,t)$ at the system boundaries. In particular, for the wind tunnel model, the drive motors and the inlet guide vane systems impose dynamic constraints on the compressor speed and the inlet guide vane flap angle. In particular, the torque equation for the drive motors is as follows:

$$\dot{\omega} = \frac{a_m R_r (\omega_s - \omega)}{b_m (\omega_s - \omega)^2 + c_m R_r (\omega_s - \omega) + d_m R_r^2} - e_m [p_0(0,t) - p_0(L,t)] \tag{97}$$

where R_r is a rotor resistance which controls the motor drive speed; ω_s is the synchronous speed; and a_m, b_m, c_m, d_m, and e_m are some parameters.

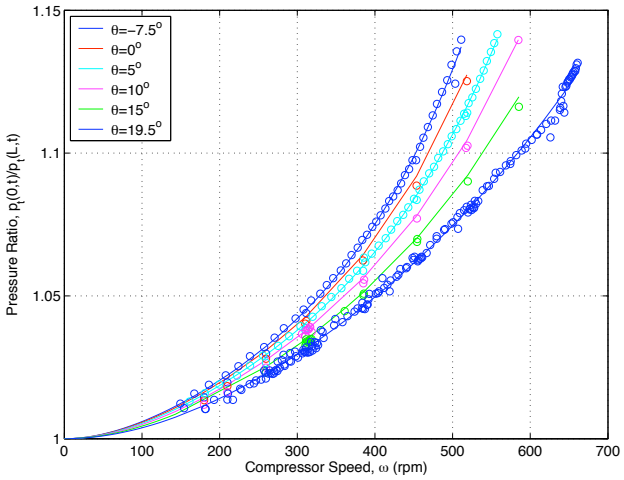

Fig. 5 - Compressor Pressure Ratio

Similarly, the dynamics of the inlet guide vane system is described by the following equation

$$\dot{\theta} = q(L,t)(a_i \theta + b_i) + c_i V_a \tag{98}$$

where V_a is a field voltage that controls the inlet guide vane system; and a_i, b_i, and c_i are some parameters.

In the context of Eq. (27), the boundary control vector $\mathbf{u} = \begin{bmatrix} \omega & \theta \end{bmatrix}^T$ is dynamically constrained by Eqs. (97) and (98) and is controlled by the auxiliary control vector $\mathbf{v} = \begin{bmatrix} R_r & V_a \end{bmatrix}^T$.

B. Results

A simulation is conducted to compute the test section Mach number transition from Mach 0.6 to Mach 0.9 in the 11-Ft TWT. The wind tunnel model is discretized into 221 nodes as shown in Fig. 6.

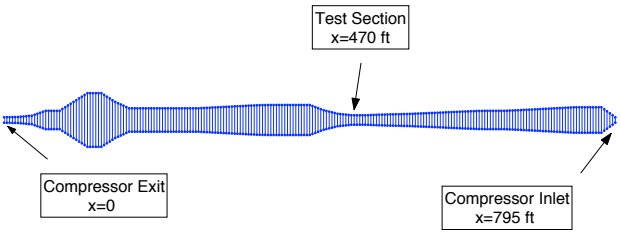

Fig. 6 - Wind Tunnel Discretization

The step size $\Delta x = 3.6$ ft is chosen so that important features of the wind tunnel such as the aftercooler and test section positions are captured in the spatial discretization. The simulation time for the Mach number transition is about 2 minutes. The time step $\Delta t = 0.001$ sec is used in order to satisfy the CFL condition (72). The time histories of the compressor speed and the inlet guide vane flap angle during the Mach number transition from 0.6 to 0.9 are plotted in Fig. 7. The transition takes place over a 120-sec interval. At the beginning of the transition, the inlet guide vane flap angle is adjusted while the compressor speed is held constant at 455 rpm. A new compressor speed set point of 590 rpm is then sought while the inlet guide vane flap angle is maintained constant at 19.5°. Once the compressor speed is stabilized, the inlet guide vane flap angle is adjusted in a closed-loop feedback mode using the test section Mach number error as a feedback variable. The ripples at the beginning of the final interval are due to a compressor speed proportional and integral feedback control implemented in the simulation.

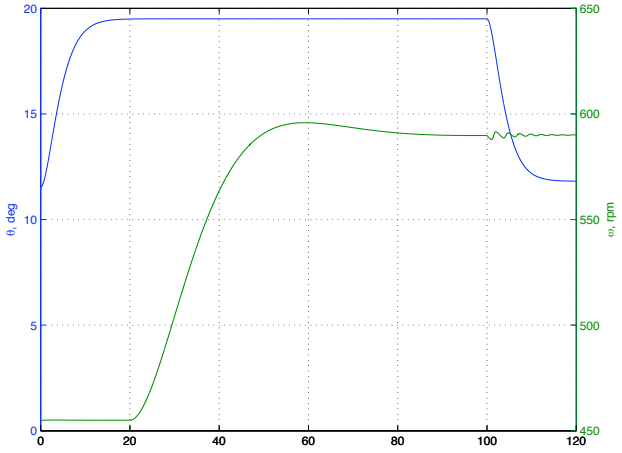

Fig. 7 - Compressor Speed and Inlet Guide Vane Flap Angle Responses

The corresponding inlet guide vane field voltage and the drive motor rotor resistance that control the motion of the compressor speed and the inlet guide vane flap angle are plotted in Fig. 8.

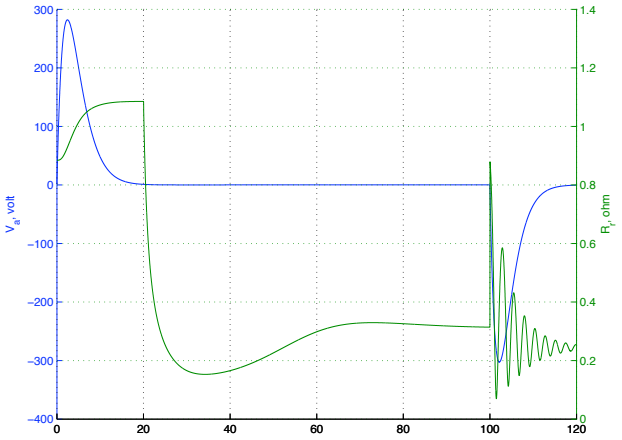

Fig. 8 - Drive Motor Rotor Resistance and Inlet Guide Vane Motor Voltage

Fig. 9 illustrates the test section Mach number response computed using the wave-splitting finite-difference method as compared with the wind tunnel test data. An excellent agreement between the computed test section Mach number and the test data is observed.

The complete solution of the Euler equations are plotted in Figs. 10 to 13. The Mach number distribution in the wind tunnel is shown in Fig. 10, showing the peaked Mach number in the test section. Elsewhere in the wind tunnel, the Mach number is nominal low and in the upper incompressible range below a Mach number of 0.35. The mass flow distribution in the wind tunnel is plotted in Fig. 11. It can be seen that the mass flow is essentially constant at all locations in the wind tunnel.

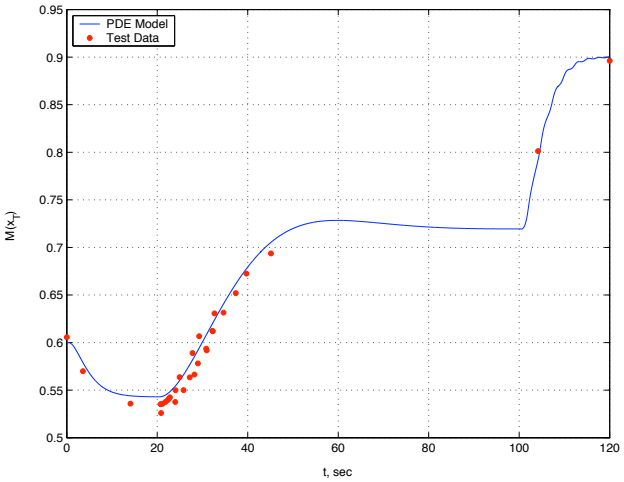

Fig. 9 - Test Section Mach Number Response

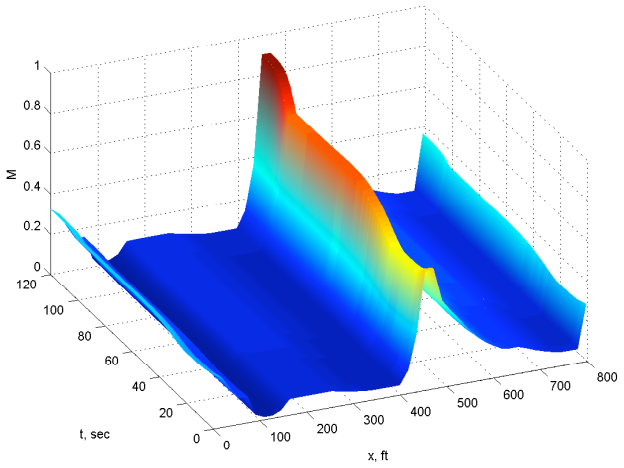

Fig. 10 - Mach Number Distribution

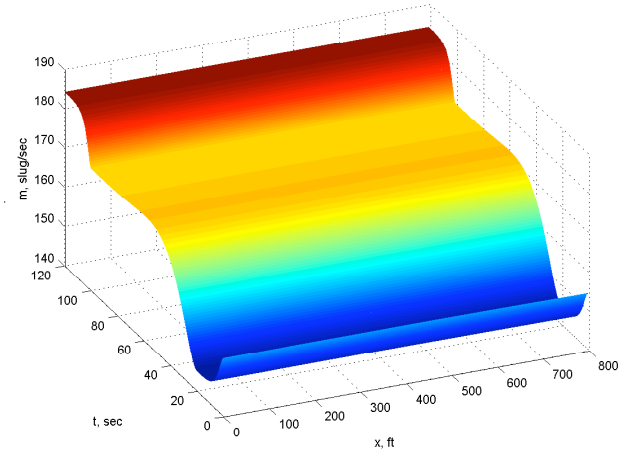

Fig. 11 - Mass Flow Distribution

Fig. 12 is a plot of the stagnation pressure distribution in the wind tunnel. It is always decreasing in the x-direction due to viscous losses in the flow. The stagnation temperature distribution is plotted in Fig. 13. It can be seen that the stagnation temperature is almost constant throughout the wind tunnel except in the region between the compressor exit and the aftercooler where the heat transfer process takes place. As the Mach number increases, the stagnation temperature at the compressor exit rises due to a greater work input from the drive motors. This work input must be removed by the aftercooler in order to maintain a stable stagnation temperature in the test section for aerodynamic testing. In reality, the work input is not always completely removed by the aftercooler especially at a high supersonic flow in the test section. However, for subsonic flow, the assumption of a perfect heat transfer is quite reasonable.

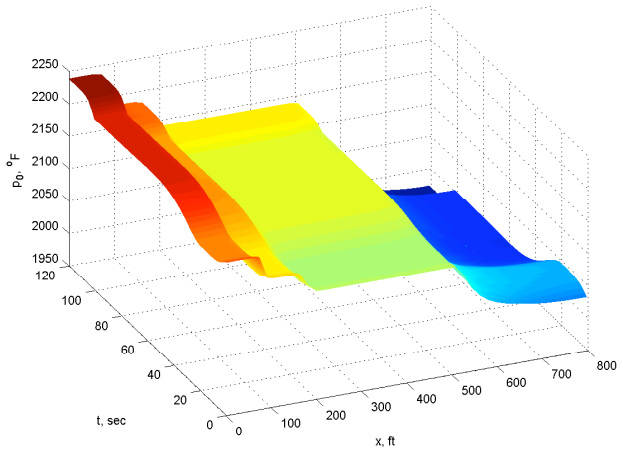

Fig. 12 - Stagnation Pressure Distribution

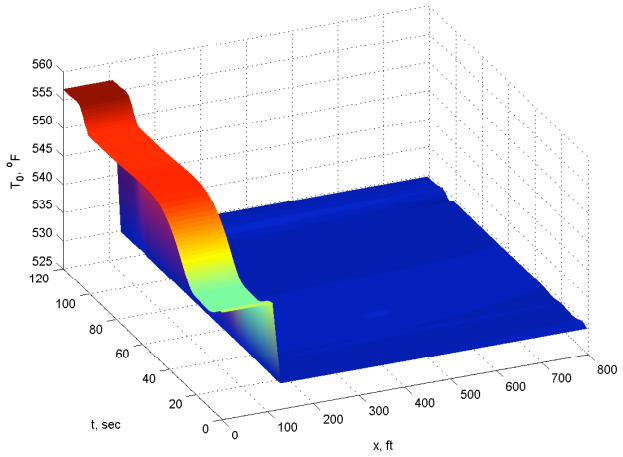

Fig. 13 - Stagnation Temperature Distribution

Fig. 14 illustrates the test section Mach number response computed by the half-point discretization of the characteristic matrices according to Eqs. (48) and (49). The agreement between the current discretization and the half-point discretization is quite good. However, it can be seen that the half-point method did not quite converge to the correct Mach number as the current method. This slight discrepancy is due to the inconsistency in the space discretization. The advantage with the current scheme is that the characteristic matrices are evaluated using only information at one grid point whereas the half-point scheme requires information at two grid points. Thus, computationally, the current method is twice as less expensive than the half-point method.

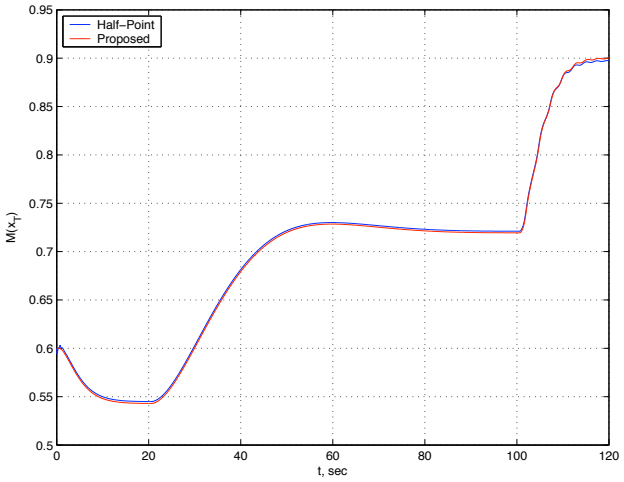

Fig. 14 - Comparison between Half-Point Discretization and Current Discretization

To demonstrate the shock capturing method, a simulation of transonic flow in the wind tunnel is conducted. The Mach number in the test section is maintained at Mach 1.2 at all times and the inlet guide vane flap angle is adjusted from 10^o to 4^o corresponding to the Mach 1.4 setting. Since the Mach number in the test section is dictated by the area ratio between the test section and the nozzle throat, without adjusting the flexible nozzle, the effect of the inlet guide vane adjustment is to cause the normal shock to move downstream of the test section. To compute the shock location, four different number of grid points are used: 401, 801, 1601, and 3201. The plots of the computed shock location are shown in Fig. 15.

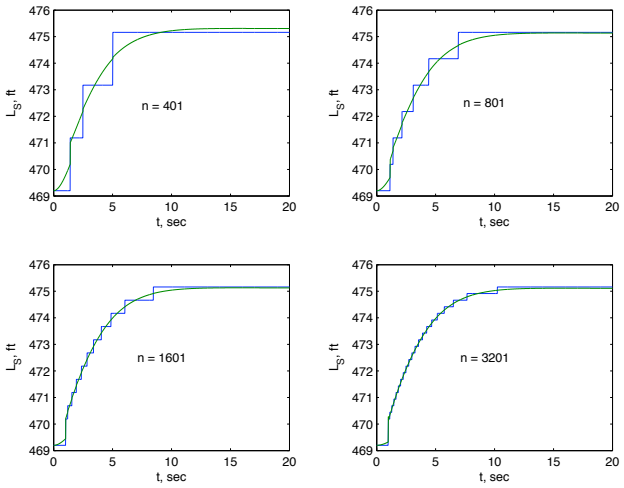

Fig. 15 - Computed Shock Location

The stair case plots are the computed shock locations at the grid points and the smooth curves are the plots of the fitted shock locations using a first-order fitting method. Fig. 16 illustrates a well-known fact that in order to accurately capture a shock location, the number of grid points must be sufficiently large. In fact, the shock location error is found to be very close to half of the Δx step size. Fig. 17 and 18 is the plot of the Mach number in the wind tunnel circuit showing the final shock location moved to downstream of the test section.

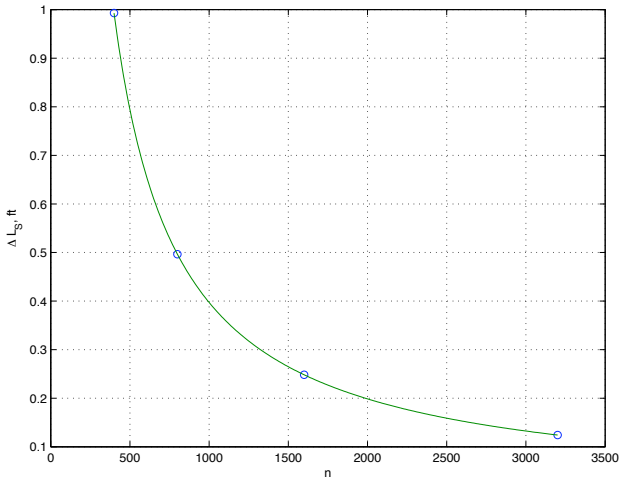

Fig. 16 - Maximum Shock Location Error vs. Number of Grid Points

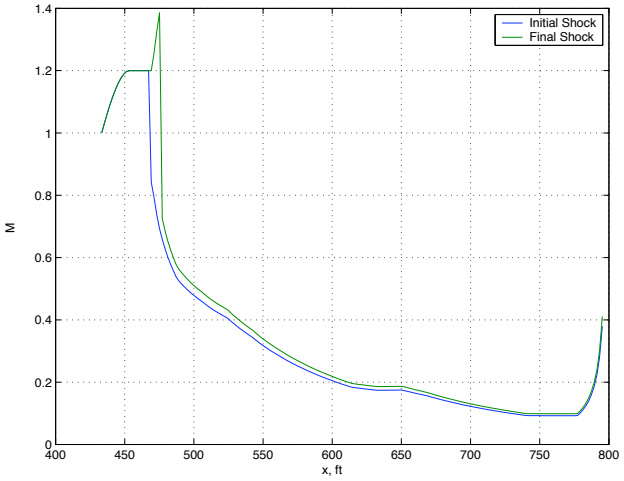

Fig. 17 - Initial and Final Mach Number Variations

V. Conclusions

This paper has presented a computational method for a closed-loop fluid transport system based on the one-dimensional unsteady Euler equations with a dissipative source term. A non-conservation form is formulated in terms of the mass flow, the stagnation pressure, and the stagnation temperature. In this form, the mass flow and the stagnation temperature are in fact conserved quantities. Therefore, the present non-conservation form represents an intermediate model between the conserved variable formulation and the primitive variable formulation. The closed-loop transport system is modeled via a nonlinear forced periodic boundary condition which in turn is coupled to a system of ordinary differential equations that model an auxiliary system which actually controls the behavior of the fluid conditions at the boundary. A wave-splitting, finite-difference upwind method is introduced. This scheme maintains a consistency with the steady state discretization. A numerical simulation of unsteady flow in a closed-circuit wind tunnel demonstrates an excellent agreement with experimental data. When compared with a half-point scheme, the present scheme shows a better convergence. A shock capturing scheme is presented for the non-conservation form. A numerical simulation shows the that shock location is very close to half of the spatial step size. Thus, to capture the shock location accurately, a sufficient number of grid points must be used.

References

[1]Rothfarb, B., Frank, H., Rosenbaum, D. M., Steiglitz, K., Kleitman, D. J., "Optimal Design of Offshore Natural-Gas Pipeline Systems", Journal of the Operations Research Society of America, Vol. 18, No. 6, December 1970, pp. 992-1020.

[2]Bayen, A. M., Raffard, R., Tomlin, C. J., "Adjoint-Based Constrained Control of Eulerian Transportation Networks: Application to Air Traffic Control", Proceeding of the 2004 American Control Conference, June 2004, pp. 5539-5545.

[3]Lee, H. Y., Lee, H.-W., Kim, D., "Dynamic States of a Continuum Traffic Equation with On-Ramp", Physical Review E, Vol. 59, No. 5, May 1999, pp. 5101-5111.

[4]Debnath, L., *Nonlinear Partial Differential Equations for Scientists and Engineers*, Birkhauser, Boston, 1997.

[5]Shapiro, A. H., *The Dynamics and Thermodynamics of Compressible Fluid Flow*, Volume II, Ronald Press Company, New York, 1954.

[6]Laney, C. B., *Computational Gas Dynamics*, Cambridge University Press, New York, 1998.

[7]Wendt, J. F., *Computational Fluid Dynamics - An Introduction*, 2nd Edition, Springer-Verlag, 1996.

[8]Hirsh, C., *Numerical Computation of Internal and External Flows*, Vol. 1, John Wiley & Sons, Brussels, 1991.

[9]Wolf, T., "State of the Art in Circuit Loss Analysis of Transonic Wind Tunnels", AIAA 20th Advanced Measurement and Ground Testing Technology Conference, Albuquerque, AIAA-1998-2779, 1998.

[10]Soeterboek, R. A. M., Pels, A. F., Verbruggen, H. B., van Langen, G. C. A., "A Predictive Controller for Mach number in a Wind Tunnel", IEEE Control Systems, Vol. 11, Issue 1, 1991, pp 63-72.

[11]Dixon, S. L., *Thermodynamics of Turbomachinery*, Pergamon Press, New York, 1989.